Original Article

MOLECULAR METABOLISM

Calponin 2 harnesses metabolic reprogramming to determine kidney fibrosis

Yuan Gui [1], Yuanyuan Wang [1], Zachary Palanza [1], Jack L. Wang [1], Priya Gupta [1], Jianling Tao [2], Yi Qiao [3], Geneva Hargis [4], Donald L. Kreutzer [3], Sheldon I. Bastacky [5], Yanbao Yu [6], Yanlin Wang [1], Silvia Liu [5], Haiyan Fu [7], Dong Zhou [1,*]

ABSTRACT

Objective: In the fibrotic kidneys, the extent of a formed deleterious microenvironment is determined by cellular mechanical forces. This process requires metabolism for energy. However, how cellular mechanics and metabolism are connected remains unclear.

Methods: A multi-disciplinary approach was employed: the fibrotic kidney disease models were induced by renal ischemia-reperfusion injury and unilateral ureteral obstruction in Calponin 2 (CNN2) knockdown mice. Proteomics, bioinformatics, and *in vivo* and *in vitro* molecular experimental pathology studies were performed.

Result: Our proteomics revealed that actin filament binding and cell metabolism are the two most dysregulated events in the fibrotic kidneys. As a prominent actin stabilizer, CNN2 was predominantly expressed in fibroblasts and pericytes. In CKD patients, CNN2 levels was markedly induced in blood. In mice, CNN2 knockdown preserves kidney function and alleviates fibrosis. Global proteomics profiled that CNN2 knockdown enhanced the activities of the key rate-limiting enzymes and regulators of fatty acid oxidation (FAO) in the diseased kidneys. Inhibiting carnitine palmitoyltransferase 1α in the FAO pathway resulted in lipid accumulation and extracellular matrix deposition in the fibrotic kidneys, which were restored after CNN2 knockdown. Bioinformatics and chromatin immunoprecipitation showed that CNN2 interactor, estrogen receptor 2 (ESR2), binds peroxisome proliferator-activated receptor-α (PPARα) to transcriptionally regulate FAO downstream target genes expression amid kidney fibrosis. *In vitro*, ESR2 knockdown repressed the mRNA levels of PPARα and the key genes in the FAO pathway. Conversely, activation of PPARα reduced CNN2-induced matrix inductions.

Conclusions: Our results suggest that balancing cell mechanics and metabolism is crucial to develop therapeutic strategies to halt kidney fibrosis.

© 2023 The Author(s). Published by Elsevier GmbH. This is an open access article under the CC BY-NC-ND license (http://creativecommons.org/licenses/by-nc-nd/4.0/).

Keywords Calponin 2; ESR2; Fatty acid oxidation; Proteomics; Chronic kidney disease

1. INTRODUCTION

Chronic kidney disease (CKD) is estimated to become the 5th leading cause of death worldwide by 2040 [1,2]. As the common consequence of CKD, kidney fibrosis refers to a heterogeneous group of disorders that scar kidneys, most often inevitably and irreversibly [3]. In fibrosis, cell mechanical forces are essential in controlling fibroblast activation and extracellular matrix (ECM) stiffness, and regulating tubular cell metabolic reprogramming for energy [4,5]. Nevertheless, mechanotransduction is often ignored in studying CKD.

Mechanical signals are equally important to chemical signals in exerting biological effects. Our proteomics data revealed that actin filament binding is a key event in kidney fibrosis. Serving as an actin stabilizer, Calponin (CNN) plays a central role in numerous fundamental processes, including cell proliferation, motility, and adhesion [6,7]. CNN mostly consists of α-helices with hydrogen bond turns. As a binding protein, CNN structure consists of three domains. These domains appear in order of CNN homology, regulatory domain, and the domain containing the CNN repeats. In the human genome, CNN has three isoforms: CNN1, CNN2, and CNN3 [6]. In comparison to CNN1 and CNN3, CNN2 is expressed in more tissues and cell types [6,8]. Under pathophysiological conditions, CNN2 deletion attenuates inflammatory arthritis [9], calcific aortic valve disease [10], postoperative peritoneal adhesions [11], and tumor metastasis [12]. However, little is known about how CNN2 influences kidney fibrosis.

Cell mechanics and metabolism are intrinsically intertwined [13]. After CKD, tubular epithelial cells (TECs), the largest resident cell population in the kidney, can adapt to the fibrotic microenvironment by reprogramming their metabolism to meet the energy consumption requirements and improve CKD [14,15]. Importantly, this metabolic reprogramming provides energy for actin cytoskeletal rearrangement in response to external forces [16]. TECs demand high energy which

[1]Division of Nephrology, Department of Medicine, University of Connecticut School of Medicine, Farmington, CT, 06030, USA [2]Division of Nephrology, Department of Medicine, Stanford University School of Medicine, Stanford, CA, 94305, USA [3]Department of Surgery, University of Connecticut School of Medicine, Farmington, CT, 06030, USA [4]University of Connecticut, School of Medicine, Farmington, CT, 06030, USA [5]Department of Pathology, University of Pittsburgh School of Medicine, Pittsburgh, PA, 15261, USA [6]Department of Chemistry & Biochemistry, University of Delaware, Newark, DE, 19716, USA [7]State Key Laboratory of Organ Failure Research, National Clinical Research Center of Kidney Disease, Division of Nephrology, Nanfang Hospital, Southern Medical University, Guangzhou, 510515, China

*Corresponding author.Division of Nephrology, Department of Medicine, University of Connecticut School of Medicine, 263 Farmington Ave, L1062, Farmington, CT 06030, USA. E-mail: dzhou@uchc.edu (D. Zhou).

Received January 9, 2023 • Revision received March 6, 2023 • Accepted March 16, 2023 • Available online 22 March 2023

https://doi.org/10.1016/j.molmet.2023.101712

 © 2023 The Author(s). Published by Elsevier GmbH. This is an open access article under the CC BY-NC-ND license (http://creativecommons.org/licenses/by-nc-nd/4.0/).

primarily relies on fatty acid oxidation (FAO) and mitochondrial oxidative phosphorylation to generate adenosine triphosphate (ATP) as their energy source [17]. Under CKD, defective FAO induces intracellular lipid accumulation and ATP depletion. Consequently, cellular lipotoxicity and energy deprivation contribute to TEC dedifferentiation, leading to irreversible kidney fibrosis [18–20]. Fatty acid (FA) is transported to the kidney mainly by the cluster of differentiation 36 (CD36) or FA transporter 2 [21,22]. It is then catalyzed to fatty acyl-CoA by acyl-CoA synthetase (Acsm) in cells [23]. Activated FA enters the mitochondrial matrix for β-oxidation mediated by carnitine palmitoyltransferase 1 (CPT1) and 2 (CPT2) [24]. In mitochondria, key rate-limiting enzymes such as CPT1, peroxisomal acyl-CoA oxidase (ACOX), acyl-CoA dehydrogenase medium chain (Acadm) or long chain (Acadl) are required to degrade fatty acyl-CoA into the end-product, acetyl-CoA, by FA β-oxidation [25]. Lastly, acetyl-CoA enters the tricarboxylic acid (TCA) cycle to generate ATP [26]. Peroxisome proliferator-activated receptor α (PPARα) transcriptionally controls expression of FAO genes to balance FA uptake and oxidation and determine CKD outcomes [15,20,27]. Because epithelial-mesenchymal communication is key for controlling CKD progression [28], we hypothesized that CNN2 affects the FAO pathway and causes kidney fibrosis. Understanding cellular mechano-metabolic changes will create therapeutic opportunities to treat CKD.

2. MATERIALS AND METHODS

Detailed methods are in the Supplementary Materials.

2.1. Mouse models of CKD

Male Balb/c mice were obtained from the Jackson Laboratory. Mouse CKD models were induced by ischemia-reperfusion injury (IRI), unilateral ureteral obstruction (UUO), and adriamycin (ADR), as described previously [29,30]. Customized short hairpin RNA (ShRNA) specific for the mouse CNN2 gene was ordered from Qianlong Biotech. In a separate experiment, etomoxir was administrated in mice 2 days before IRI and nephrectomy, respectively. All animal experiments were approved by the Institutional Animal Care and Use Committee at the University of Connecticut, School of Medicine.

2.2. Human kidney biopsy specimens

Human kidney biopsy specimens and non-tumor kidney tissue were obtained from the pathology archive at the University of Pittsburgh Medical Center. All procedures followed ethical standards and were approved by the Institutional Review Board at the University of Pittsburgh, School of Medicine. Demographic data are in Supplementary Table S1.

2.3. Proteomic analysis

Kidney tissues were processed following a shotgun proteomics workflow published previously [31]. The LC-MS/MS analysis was performed using an Ultimate 3000 nanoLC and Q Exactive mass spectrometer system.

2.4. Determination of blood urea nitrogen (BUN), serum creatinine (Scr), and alanine transaminase (ALT)

BUN, Scr, and ALT levels were determined respectively using the QuantiChrom™ Urea, Creatinine, and ALT assay kits, according to the protocols specified by the manufacturer.

2.5. Quantitative real-time reverse transcription PCR (qRT-PCR)

Total RNA isolation and qRT-PCR were conducted by procedures described previously [29]. The mRNA levels of various genes were calculated after normalizing with β-actin or GAPDH. The primer sequences used are in Supplementary Table S2.

2.6. Western blot analysis

Protein expression was analyzed by western blot as described previously [29]. Antibodies used are in Supplementary Table S3.

2.7. Triglyceride and ATP measurement

The levels of serum, kidney, and liver triglyceride or kidney ATP content were measured by using the Triglyceride Quantification Kit or the ATP Colorimetric/Fluorometric Assay Kit, according to manufacturers' instructions.

2.8. Enzyme-linked immunosorbent assay (ELISA)

The human and rat calponin 2 ELISA kits were purchased from MyBioSource, Inc. This assay employs the quantitative sandwich enzyme immunoassay technique.

2.9. Histology, and Oil Red O, immunohistochemical, and immunofluorescence staining

Paraffin-embedded kidney sections and cryosections were prepared by a routine procedure. The sections were stained with Masson Trichrome Staining reagents or Oil Red O staining reagents. Immunostaining was performed according to the established protocol as described previously [29]. Antibodies used are in Supplementary Table S3.

2.10. Cell culture, small interfering RNA (siRNA) inhibition, and treatment

Normal rat kidney fibroblasts (NRK-49F) and human proximal tubular cells (HK-2) were obtained from the American Type Culture Collection. For conditioned media (CM) collection, NRK-49F were transfected with siCNN2 for 24 h and then cultured with serum-free media for 24 h. Serum-starved HK-2 cells were then transfected with ESR2-Dicer siRNA or treated with CM, CNN2 recombinant protein, etomoxir, or fenofibrate.

2.11. Chromatin immunoprecipitation (ChIP) assay

To analyze interactions between ESR2 and the binding sites in the PPARα gene promoter, a ChIP assay was performed. This assay was conducted according to the manufacturer-specified protocols. Primer sequences used for the ChIP assay are in Supplemental Table S2.

2.12. Statistics

All data were expressed as mean ± SEM if not specified otherwise in the legends. Statistical analysis of the data was performed using GraphPad Prism 9. Results are presented in dot plots. $P < 0.05$ was considered statistically significant.

3. RESULTS

3.1. Global proteome characterization after CKD

At the genome-wide transcript level, metabolism is a key pathway in metabolic disease-associated CKD patients [19]. To investigate whether metabolism is also involved in non-metabolic disease-associated CKD, we used quantitative proteomics to profile the kidney proteome landscape of controls and IRI-induced CKD mice. The principal component analysis (PCA) showed distinct segregation of proteins in control and IRI mice kidneys (Figure 1A). Correlations between biological replicates within the same group and the distribution of protein intensity are presented (Figure 1, B–C). In total, we identified

 © 2023 The Author(s). Published by Elsevier GmbH. This is an open access article under the CC BY-NC-ND license (http://creativecommons.org/licenses/by-nc-nd/4.0/).

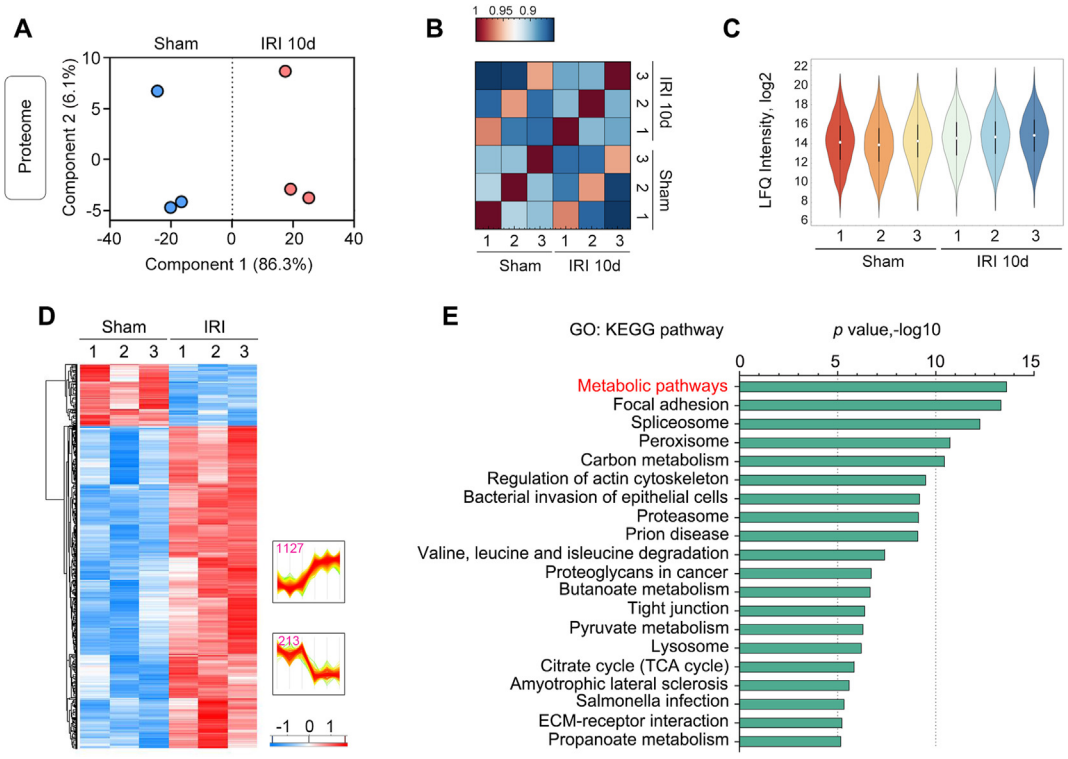

Figure 1: The landscape of proteomes in CKD. (**A**) Principal component analysis of proteomes in control and IRI-induced CKD kidneys. (**B**) Correlation of kidney proteome profiles between control and IRI-induced CKD kidneys. The color scale represents R^2 values. (**C**) Violin plot of ANOVA significant proteins (Permutation FDR 0.05) among control and IRI-induced CKD kidneys. Label-free quantitation (LFQ) intensities of represented proteins were z-scored and plotted according to the color bar. (**D**) Hierarchical clustering of the intensity (plotted as z-score) of the proteins identified in the control and ischemic kidneys by quantitative proteomic analysis. Two clusters of proteins with different patterns of abundance profiles were highlighted in the heatmap. (**E**) KEGG pathway enrichment analyses revealed the top 20 activated pathways in the ischemic kidneys after CKD.

6,146 proteins and 1,340 of these had significantly different expression (Permutation FDR 0.05) between control and ischemic kidneys (Figure 1D). Compared to controls, 1,127 and 213 proteins were up- and down-regulated in the ischemic kidneys. Kyoto Encyclopedia of Genes and Genomes (KEGG) enrichment analysis highlighted that metabolic pathways are the most significantly disturbed events (Figure 1E), consistent with the transcript-level results [19].

3.2. Calponin 2 is a key actin filament-associated regulatory protein that facilitates kidney fibrosis

Besides the disturbance of metabolic pathways, Gene Ontology (GO) analysis of molecular function revealed that protein binding, RNA binding, and actin filament binding are the top 3 events that play a key role in facilitating kidney fibrosis (Figure 2A). Considering kidney fibrosis is directly determined by cellular mechanical forces, we decided to focus our study on dissecting the role of actin filament binding in CKD. Earlier studies showed that cell mechanics and metabolism are reciprocally regulated [13], we therefore screened the significant actin filament regulatory proteins in our proteomics database. To identify the most impacted cell mechanics-related proteins for investigation, we excluded unknown proteins and those that have been well studied (Figure 2B). Among the remaining proteins, we identified CNN2 as a protein of interest (Figure 2C) because it is predominantly expressed in the cells that are physiologically under high mechanical tension, have high rates of proliferation, and are actively migrating. To enhance the reproducibility of our proteomic analyses, we constructed three well-characterized CKD models induced by IRI, UUO, and ADR, respectively. CNN2 mRNA was significantly increased in all three models' fibrotic kidneys compared to controls (Figure 2D). Western blots demonstrated CNN2 protein was upregulated in the fibrotic kidneys (Figure 2E and Supplementary Figure S1, A-C). A separate single-nucleus RNA sequencing revealed that CNN2 was mainly expressed by kidney fibroblasts and pericytes after 14 days of IRI (Figure 2F) [32]. Consistently, immunohistochemical staining confirmed that CNN2 was predominantly localized in the fibrotic kidney interstitium (Figure 2G). Using double immunostaining for CNN2 (red) and fibroblast/pericyte marker platelet-derived growth factor receptor β (PDGFRβ, green), we confirmed that fibroblasts/pericytes are the major sources of CNN2 in the fibrotic kidneys after IRI (Figure 2H).

To establish the clinical relevance of CNN2 expression in human CKD, we immunohistochemically stained kidney biopsy specimens from CKD patients with different etiologies for CNN2. CNN2 was induced in the interstitium of all CKD patients, compared with non-tumor HA controls (Figure 2I and Supplementary Figure S1D). To determine whether CNN2 is detectable in circulation, we further analyzed serum CNN2 level from 75 healthy adults and 84 non-diabetic CKD patients and found it was increased in CKD patients (Figure 2J).

3.3. CNN2 knockdown alleviates kidney fibrosis

To explore the role of CNN2 in kidney fibrosis, we employed a hydrodynamic gene delivery technique to knock down CNN2 in IRI and UUO models (Figure 3A and Supplementary Figure S2A). Compared to vehicles, qPCR and western blot analyses confirmed that CNN2 induction was reduced in the fibrotic kidneys of ShCNN2 mice (Figure 3, B—C; Supplementary Figure S2, B—C and S3A). Immunohistochemical staining and double staining for CNN2 (red) and PDGFRβ (green)

 © 2023 The Author(s). Published by Elsevier GmbH. This is an open access article under the CC BY-NC-ND license (http://creativecommons.org/licenses/by-nc-nd/4.0/).

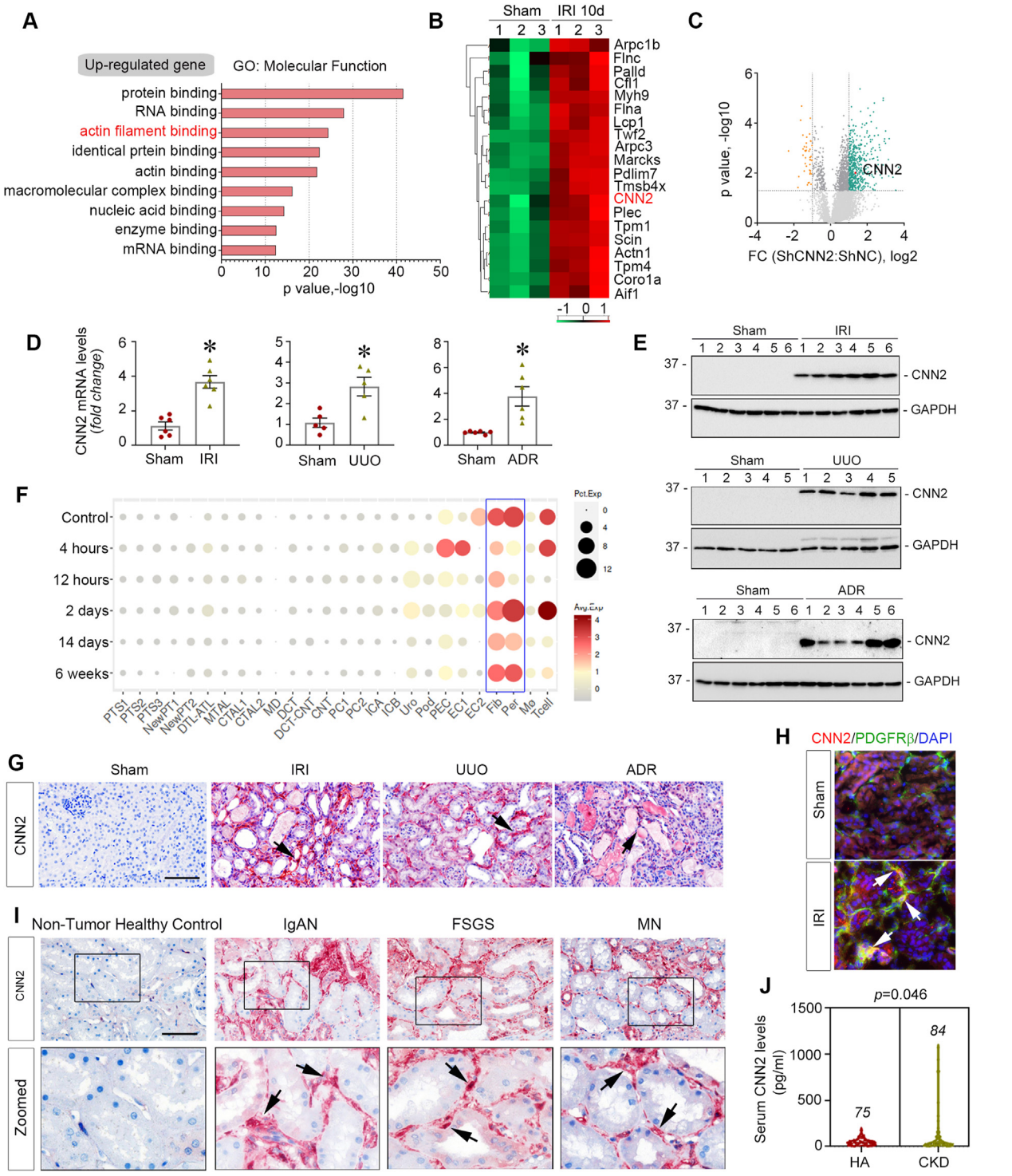

Figure 2: Calponin 2 is a key actin filament-associated regulatory protein identified in the fibrotic kidneys. (**A**) Gene Ontology (GO) enrichment analysis revealed that actin filament binding is listed as one of the top 3 significantly upregulated events under molecular function terms. (**B**) Heatmap of the differentially expressed actin filament-associated regulatory proteins between controls and CKD induced by IRI. (**C**) Volcano plot showed calponin 2 (CNN2) is upregulated in the ischemic kidneys after CKD. (**D**) Quantitative RT-PCR analysis revealed that *CNN2* mRNA levels were upregulated in the fibrotic kidneys induced by IRI, UUO, and ADR nephropathy, respectively. Graphs are presented as means ± SEM. $^{*}P < 0.05$ (n = 5–6). (**E**) Western blot assays demonstrated the expression of CNN2 protein in the fibrotic kidneys induced by IRI, UUO, and ADR nephropathy. Numbers indicate individual animals within each group. (**F**) Single nucleus RNA sequencing showed CNN2 mainly expressed by fibroblasts (Fib) and pericytes (Per) after IRI. (Data were extracted from the online database provided by Dr. Benjamin Humphrey's laboratory at the Washington University in St. Louis, http://humphreyslab.com/SingleCell/displaycharts.php). (**G**) Immunohistochemical staining showed CNN2 distributions in the fibrotic kidneys after IRI, UUO, and ADR nephropathy, respectively. (**H**) Immunofluorescence staining demonstrated the co-staining of CNN2 (red) and platelet-derived growth factor receptor β (green) in the ischemic kidneys. (**I**) Representative immunohistochemical staining images showed CNN2 expression in the non-tumor normal human kidneys and the kidney biopsy specimens from CKD patients diagnosed with IgA nephropathy (IgAN), focal segmental glomerulosclerosis (FSGS), and membrane nephropathy (MN). Boxed areas are zoomed. (**J**) Serum CNN2 levels in healthy adults (n = 75) and non-diabetic CKD patients (n = 84). Graphs are presented as means ± SEM. Arrows indicate positive staining. Scale bar, 50 μm. IRI, ischemia reperfusion injury; UUO, unilateral ureteral obstruction; ADR, Adriamycin.

 © 2023 The Author(s). Published by Elsevier GmbH. This is an open access article under the CC BY-NC-ND license (http://creativecommons.org/licenses/by-nc-nd/4.0/).

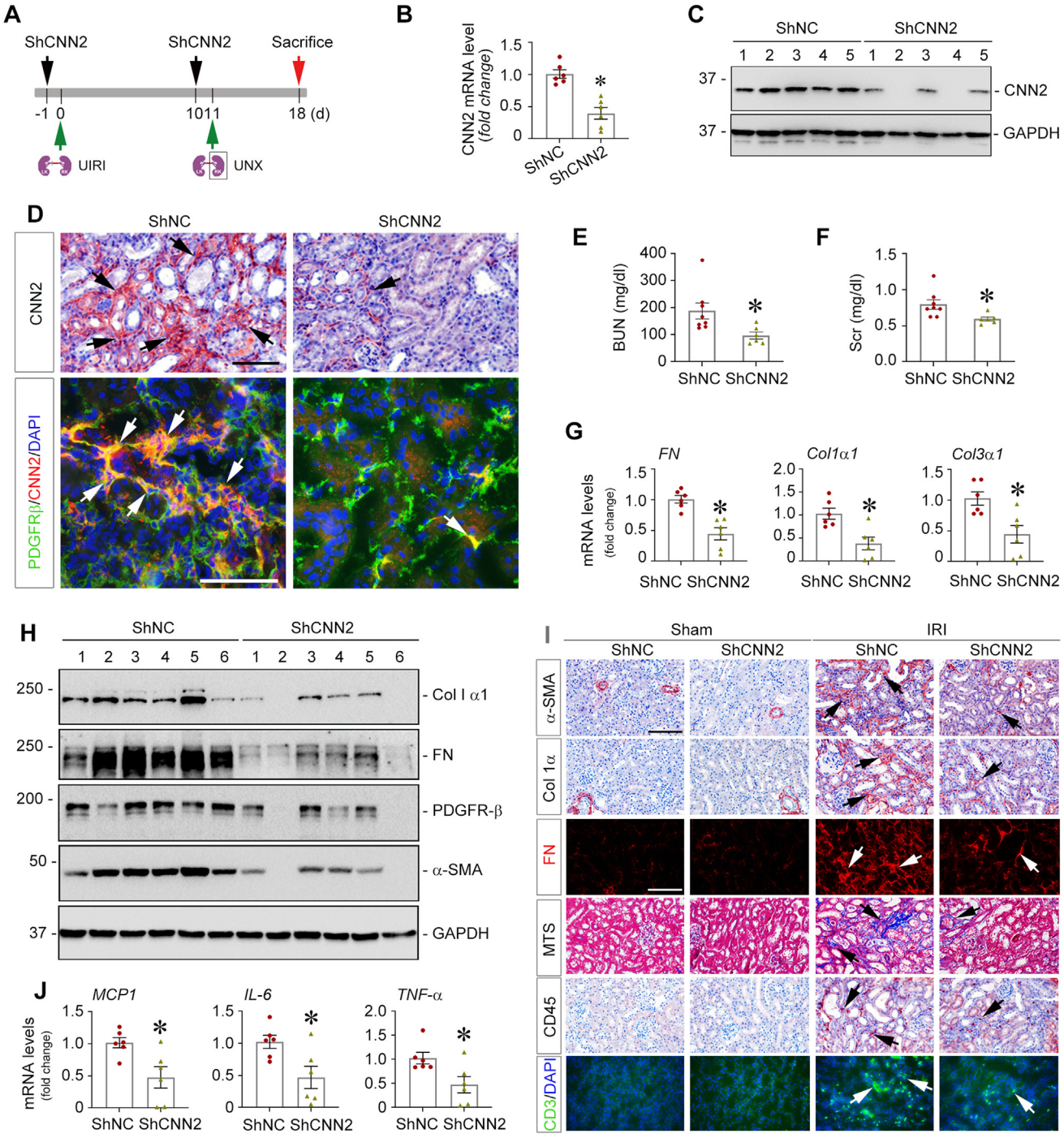

Figure 3: Knockdown of CNN2 alleviates kidney fibrosis. (**A**) Experiment design. The first dose of ShCNN2 plasmid was administrated in mice 1 day (d) before unilateral IRI (UIRI) surgery. At d10 after IRI (1d before unilateral nephrectomy, UNX), the second dose of ShCNN2 plasmid was injected. The mice were sacrificed on d18. (**B**) Quantitative RT-PCR (qPCR) analysis showed the changes of *CNN2* mRNA levels in the kidneys of ShNC and ShCNN2 mice after IRI. Graphs are presented as means ± SEM. $^*P < 0.05$ (n = 6). (**C**) Western blot assay demonstrated CNN2 protein expression in the kidneys of ShNC and ShCNN2 mice after IRI. Numbers indicate individual animals within each group. (**D**) Immunohistochemical staining and immunofluorescence co-staining of CNN2 (red) and platelet-derived growth factor receptor β (green) showed CNN2 expression and distribution in the kidneys of ShNC and ShCNN2 mice after IRI. Scale bar, 50 μm. (**E, F**) Blood urea nitrogen (BUN) and serum creatinine (Scr) levels in ShNC and ShCNN2 mice after IRI. Graphs are presented as means ± SEM. $^*P < 0.05$ (n = 6–8). (**G**) qPCR analyses revealed the mRNA abundance of *FN*, *α1 type I collagen (Col1α1)*, and *α1 type III collagen (Col3α1)* in the kidneys of ShNC and ShCNN2 mice after IRI. Graphs are presented as means ± SEM. $^*P < 0.05$ (n = 6). (**H**) Western blot assay demonstrated Col1α1, FN, α-smooth muscle actin (α-SMA), and platelet-derived growth factor receptor β (PDGFRβ) protein expression in the kidneys of ShNC and ShCNN2 mice after IRI. Numbers indicate individual animals within each group. Graphs are presented as means ± SEM. $^*P < 0.05$ (n = 6). (**I**) Representative micrographs for α-SMA, Col1α1, FN staining, Masson Trichrome Staining, CD45, and CD3 in the fibrotic kidneys of ShNC and ShCNN2 mice after IRI-induced CKD. Arrows indicate positive staining. Scale bar, 50 μm. (**J**) qPCR analyses revealed the mRNA abundance of *monocyte chemoattractant protein-1* (*MCP1*), *interleukin 6* (*IL-6*), and *tumor necrosis factor α* (*TNF-α*) in the kidneys of ShNC and ShCNN2 mice after IRI. Graphs are presented as means ± SEM. $^*P < 0.05$ (n = 6).

 © 2023 The Author(s). Published by Elsevier GmbH. This is an open access article under the CC BY-NC-ND license (http://creativecommons.org/licenses/by-nc-nd/4.0/).

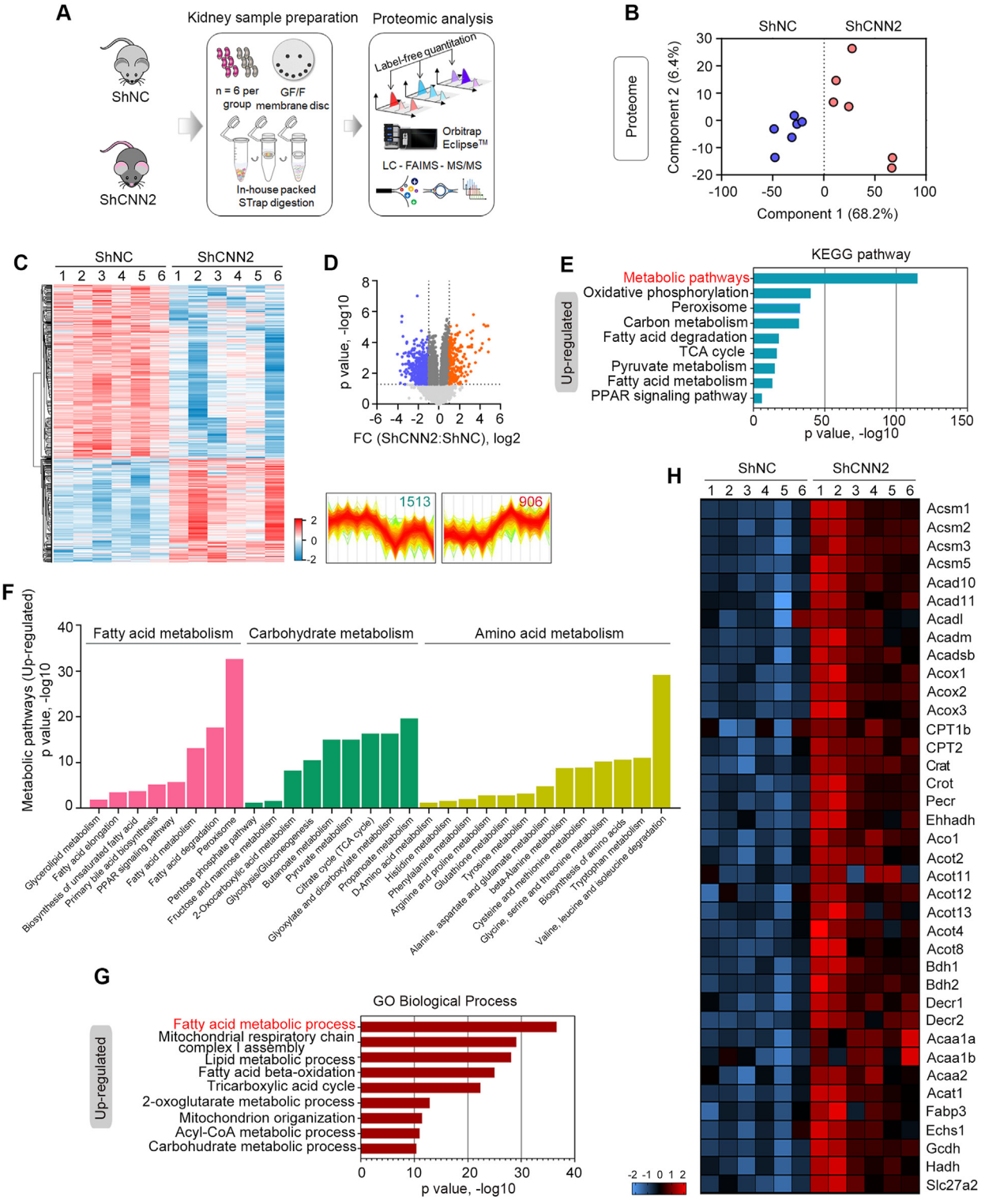

Figure 4: Global proteomics reveals fatty acid oxidation is a key pathway in mediating kidney fibrosis after knockdown of CNN2. (**A**) Experimental workflow of the global proteomic analysis. In each group, kidney samples from six mice were used for mass spectrometry. (**B**) Principal component analysis of global proteomes from ShNC and ShCNN2 fibrotic kidneys after IRI. (**C**) Heatmap of t-test significant proteins (Permutation FDR 0.05). Two clusters of proteins with different patterns of abundance profiles are highlighted in the heatmap. (**D**) Volcano plot showed the differential proteins (Permutation FDR 0.05) between ShNC and ShCNN2 fibrotic kidneys. Up- and down-regulated proteins (fold-change, FC) are colored in red and blue, respectively. (**E, F**) Kyoto Encyclopedia of Genes and Genomes (KEGG) pathway enrichment analysis highlighted upregulated metabolic pathways in fibrotic kidneys from ShNC and ShCNN2 mice after IRI. (**G**) Gene Ontology (GO) biological process terms in each cluster of proteins are plotted with their names and significance. The fatty acid metabolic process is highlighted to indicate the group with the largest difference in upregulated proteins. (**H**) Heatmap of the differentially expressed proteins in the fatty acid oxidation pathway in ShNC and ShCNN2 mice fibrotic kidneys after IRI.

 © 2023 The Author(s). Published by Elsevier GmbH. This is an open access article under the CC BY-NC-ND license (http://creativecommons.org/licenses/by-nc-nd/4.0/).

consistently showed decreased CNN2 in fibroblasts/pericytes from the fibrotic kidneys (Figure 3D and Supplementary Figure S2D). Then, we examined whether knockdown of CNN2 could preserve kidney function and alleviate kidney fibrosis. After IRI, BUN and Scr levels were reduced (Figure 3, E—F), and expression of fibrosis-related genes, including fibronectin (*FN*), α1 type I collagen (*Col1α1*), and α1 type III collagen (*Col3α1*), were reduced in ShCNN2 kidneys compared to vehicles (Figure 3G). Western blots assay demonstrated reductions of Col1α1, FN, α-smooth muscle actin (α-SMA), and PDGFRβ in ShCNN2 kidneys (Figure 3H and Supplementary Figure S3B). Immunohistochemical staining illustrated that CNN2 knockdown repressed α-SMA + myofibroblast activation, Col1α1 deposition, and FN inductions (Figure 3I and Supplementary Figure S3C). Consistently, Masson trichrome staining (MTS) showed reduced ECM deposition in ShCNN2 kidneys. Furthermore, qPCR analysis revealed decreased mRNA levels of secreted cyto-chemokines including monocyte chemoattractant protein-1 (*MCP-1*), interleukin 6 (*IL-6*), and tumor necrosis factor-α (*TNF-α*) in ShCNN2 kidneys (Figure 3J). Immunostaining showed fewer CD45+ monocytes and CD3+ T cells in ShCNN2 kidneys (Figure 3I and Supplementary Figure S3D). Consistent with the IRI model, knockdown of CNN2 exhibited similar effects on reducing ECM deposition and inflammation in a separated UUO model (Supplementary Figure S2, E-L).

3.4. Global proteomics reveals FAO is a key pathway after CNN2 knockdown

To better understand the molecular mechanisms of how knockdown of CNN2 alleviates CKD, we employed a label-free quantitative approach to profile the proteome landscape of ShNC and ShCNN2 kidneys (Figure 4A). PCA classified ShNC and ShCNN2 kidneys according to their genotype (Figure 4B). A t-test identified 2419 differentially expressed proteins (Permutation FDR 0.05) between ShNC and ShCNN2 mice. Compared to ShNC kidneys, 906 and 1513 proteins were up- and down-regulated in ShCNN2 kidneys (Figure 4, C-D and Supplementary Table S4). The proteomic measurements were reproducible as the protein intensity distribution was similar and the Pearson correlation of the six biological replicates of each group was 0.95 or higher (Supplementary Figure S4, A-B). GO and KEGG enrichment analysis revealed that the metabolic pathway was significantly upregulated in ShCNN2 fibrotic kidneys and FA metabolic process was the most changed event (Figure 4, E—G). KEGG also identified the downregulated pathways and biological processes (Supplementary Figure S4, C-D). We further investigated the dysregulated metabolic pathways. Among the FA, carbohydrate, and amino acid metabolisms, peroxisome, propanoate, and branched-chain amino acid metabolisms were significantly enriched (Figure 4F). Impressively, about 40 components in the FAO pathway, including Acsm, Acox, and CPT, were simultaneously upregulated in ShCNN2 kidneys compared to ShNC (Figure 4H).

3.5. CNN2 modifies lipid accumulation and FAO pathway activity in fibrotic kidneys

We then validated FAO regulation in ShNC and ShCNN2 kidneys. First, we examined the extent of lipid accumulation in fibrotic kidneys. Triglyceride content in sera or kidneys was decreased in ShCNN2 mice compared to ShNC after IRI (Figure 5, A—B). Oil red O staining consistently showed less triglyceride in ShCNN2 kidney tubules (Figure 5C). To enhance the evidence of lipid accumulation in the fibrotic kidneys, we employed an additional marker for lipid droplets, perilipin 2 (Plin2) [33,34]. Western blots demonstrated that Plin2 is dramatically decreased in ShCNN2 kidneys compared to ShNC (Figure 5D and Supplementary Figure S5A). Immunohistochemical staining revealed that Plin2 was predominantly distributed in ShNC kidney tubules (Figure 5E). Interestingly, although the liver is the central organ that controls lipid homeostasis, we did not observe significant differences of liver function changes and lipid accumulation in liver between ShNC and ShCNN2 mice after systemically knockdown CNN2 in IRI-induced CKD (Supplementary Figure S6, A-B).

Because FAO is the key contributor to intracellular ATP levels in tubular cells, we detected ATP consumption in the fibrotic kidneys. ELISA showed the ATP levels were higher in ShCNN2 kidneys than ShNC (Figure 5F). Then, we further examined expression of key elements in the FAO pathway in ShNC and ShCNN2 kidneys. qPCR analyses showed that a key transcriptional regulator of FAO, *PPARα*, was upregulated in ShCNN2 kidneys compared to ShNC (Figure 5G). Meanwhile, the key rate-limiting enzymes of FAO, including *CPT1α*, *Acox1-3*, *Acsm1*, *Acsm2*, *Acsm5*, *Acadm*, and *Acadl* were also increased in ShCNN2 kidneys. Western blots confirmed upregulation of PPARα and PPARγ coactivator-1α (PGC-1α) in ShCNN2 kidneys. The downstream targets, including CPT1α, Acox1, Acsm5, and Acadm were accordingly increased (Figure 5H and Supplementary Figure S5B). Immunohistochemical staining consistently showed upregulation of PPARα, CPT1α, Acox1, and Acadm in ShCNN2 kidney tubules (Figure 5I). However, after CKD, the FAO pathway activity in liver has minor changes between ShNC and ShCNN2 mice (Supplementary Figure S6, C-D). Additionally, knockdown of CNN2 also reduced lipid accumulation and FAO defect in the UUO model (Supplementary Figure S7).

3.6. CNN2 enhances CPT1α to preserve kidney function after CKD

To further elucidate how FAO impacts CKD, we applied etomoxir to specifically inhibit CPT1α, the key rate-limiting enzyme in the FAO pathway (Figure 6A). At mRNA and protein levels, etomoxir repressed CPT-1α expression, but knockdown of CNN2 restored its induction (Figure 6, B—C and Supplementary Figure S8A). As predicted, etomoxir increased BUN and Scr levels after IRI. However, after etomoxir treatment, knockdown of CNN2 preserved kidney function (Figure 6D—E). Oil Red O and immunohistochemical staining for Plin2 showed reduced lipid droplet accumulation in ShCNN2 kidney tubules compared to ShNC after etomoxir treatment (Figure 6F). Then, we further assessed the extent of kidney fibrosis. qPCR analysis revealed etomoxir increased the mRNA levels of *FN*, *Col1α1*, and *Col3α1* after IRI, but knockdown of CNN2 repressed their abundances (Figure 6G). Western blots demonstrated that etoxomir induced FN and α-SMA but knockdown of CNN2 suppressed their expression (Figure 6H and Supplementary Figure S8B). Immunostaining and MTS showed consistent results on myofibroblast activation and ECM deposition (Figure 6I and Supplementary Figure 8C). Additionally, knockdown of CNN2 reduced cyto-chemokine secretion, including *MCP-1*, *IL-6*, and *TNF-α*, and infiltration of CD45+ monocytes in IRI-induced CKD after etomoxir treatment (Supplementary Figure S8, D-F).

3.7. CNN2 knockdown promotes ESR2 binding to PPARα to enhance transcription of FAO genes

Given that CNN2 knockdown affected multiple FAO genes and its regulator PPARα expression (Figure 5), we hypothesized that there is a common mechanism that controls their activation, so we performed bioinformatics analyses. Based on GeneMANIA database, the human protein—protein network analysis indicated that estrogen receptor 2 (ESR2) is a strong interactor of CNN2 (Figure 7A). qPCR analyses showed that *ESR2* mRNA were increased in ShCNN2 kidneys compared to ShNC after IRI and UUO (Figure 7B and Supplementary Figure S9A). Western blots demonstrated increased ESR2 induction in ShCNN2 kidneys

 © 2023 The Author(s). Published by Elsevier GmbH. This is an open access article under the CC BY-NC-ND license (http://creativecommons.org/licenses/by-nc-nd/4.0/).

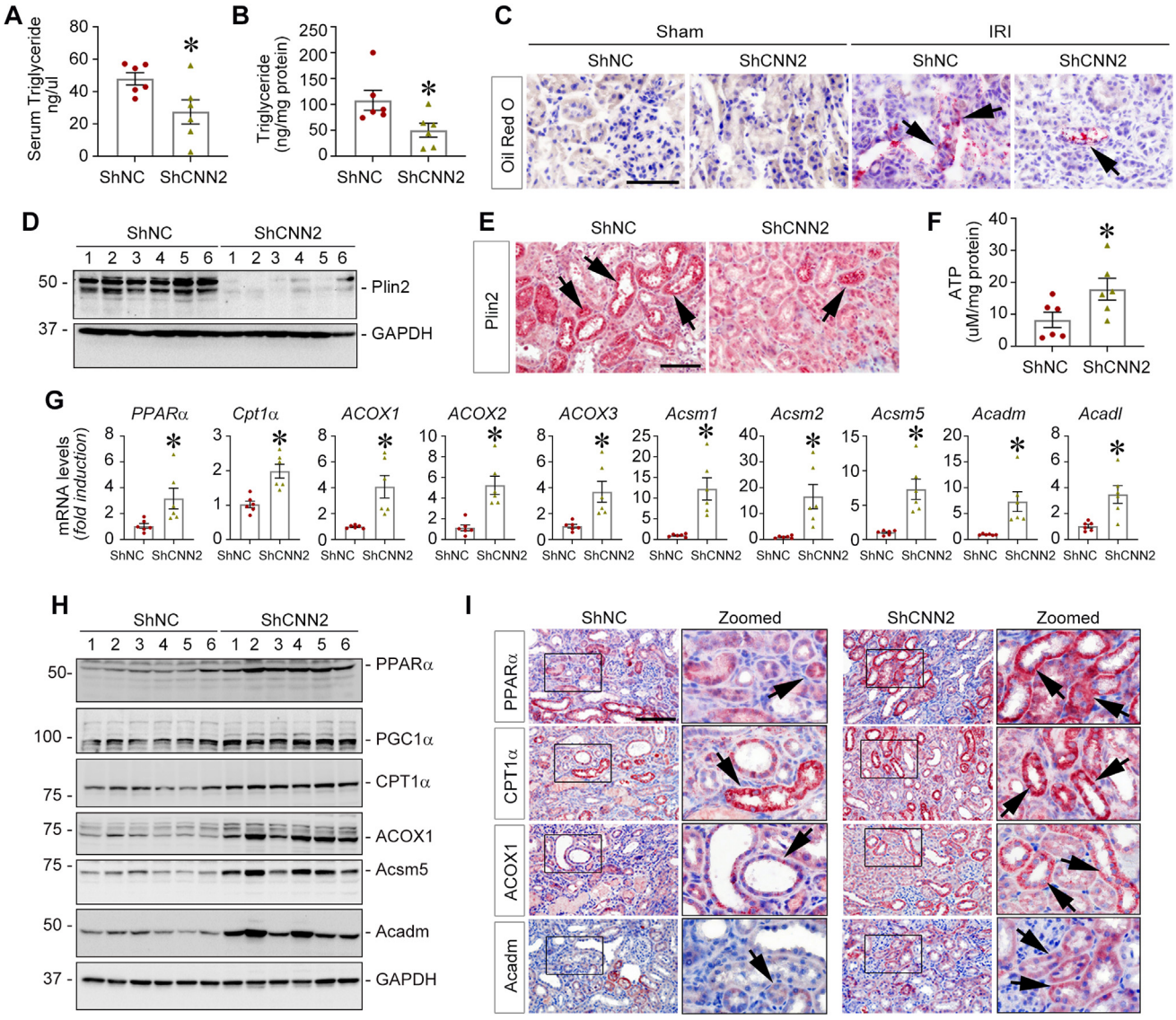

Figure 5: CNN2 modifies lipid accumulation and fatty acid oxidation pathway amid kidney fibrosis. (**A, B**) The enzyme-linked immunosorbent assay (ELISA) showed triglyceride contents in serum (**A**) and kidney (**B**) collected from ShNC and ShCNN2 mice after IRI. Graphs are presented as means ± SEM. $^*P < 0.05$ (n = 6). (**C**) Representative micrographs of Oil Red-O staining in the fibrotic kidneys from ShNC and ShCNN2 mice after IRI. Arrows indicate lipid accumulation in tubules. Scale bar, 50 μm. (**D**) Western blot assay demonstrated perilipin 2 (Plin2) protein expression in ShNC and ShCNN2 mice fibrotic kidneys after IRI. Numbers indicate individual animals within each group. (**E**) Immunohistochemical staining showed Plin2 distributions in the fibrotic kidneys of ShNC and ShCNN2 mice after IRI. Arrows indicate positive staining. Scale bar, 50 μm. (**F**) ELISA showed ATP levels in the total kidneys collected from ShNC and ShCNN2 mice after IRI. Graphs are presented as means ± SEM. $^*P < 0.05$ (n = 6). (**G**) Quantitative RT-PCR analyses revealed the mRNA abundance of *PPARα*, *CPT1α, ACOX1-3, Acsm1, Acsm2, Acsm5, Acadm,* and *Acadl* in fibrotic kidneys from ShNC and ShCNN2 mice after IRI. Graphs are presented as means ± SEM. $^*P < 0.05$ (n = 6). (**H**) Western blot assays demonstrated PPARα, PGC1α, CPT1α, ACOX1, Acsm5, and Acadm protein expression in ShNC and ShCNN2 mice fibrotic kidneys after IRI. Numbers indicate individual animals within each group. (**I**) Representative micrographs of PPARα, CPT1α, ACOX1, and Acadm staining in the fibrotic kidneys from ShNC and ShCNN2 mice after IRI. Boxed areas are enlarged. Arrows indicate positive staining. Scale bar, 50 μm.

(Figure 7C and Supplementary Figure S9B). Interestingly, under TGF-β stress *in vitro,* ELISA showed that CNN2 levels in fibroblast (NRK-49F) conditioned medium (CM) were reduced after CNN2 knockdown (Figure 7D and Supplementary Figure S9C). We then employed CNN2-deprived CM and CNN2 recombinant protein to treat human kidney proximal tubular cells (HK-2) (Figure 7E). qPCR analysis revealed that *ESR2* mRNA was induced by CNN2-deprived CM but was repressed by CNN2 recombinant protein after TGF-β stimulation (Figure 7F). Western blot assays confirmed a similar trend of ESR2 expression at the protein level (Figure 7G). Because ESR2 is a member of the superfamily of nuclear receptor transcription factors, to examine whether ESR2 directly regulates PPARα, we treated HK-2 cells with an ESR2 agonist (LY500307) and then performed a chromatin immunoprecipitation (ChIP) assay using an anti-ESR2 antibody. Through the JASPAR database, we predicted there are at least 12 putative binding sites for ESR2 on the PPARα gene promoter region (Supplementary Figure S9D). The co-precipitated chromatin DNA fragments extracted from the cells were amplified by qPCR using two pairs of primers for the PPARα promoter region. We found that the ESR2 agonist promoted ESR2 binding to the putative sites on the PPARα gene promoter (Figure 7H). *In vitro*, under TGF-β stress, knockdown of ESR2 in HK-2 cells repressed PPARα at both mRNA and protein levels (Figure 7, I–J and Supplementary

 © 2023 The Author(s). Published by Elsevier GmbH. This is an open access article under the CC BY-NC-ND license (http://creativecommons.org/licenses/by-nc-nd/4.0/).

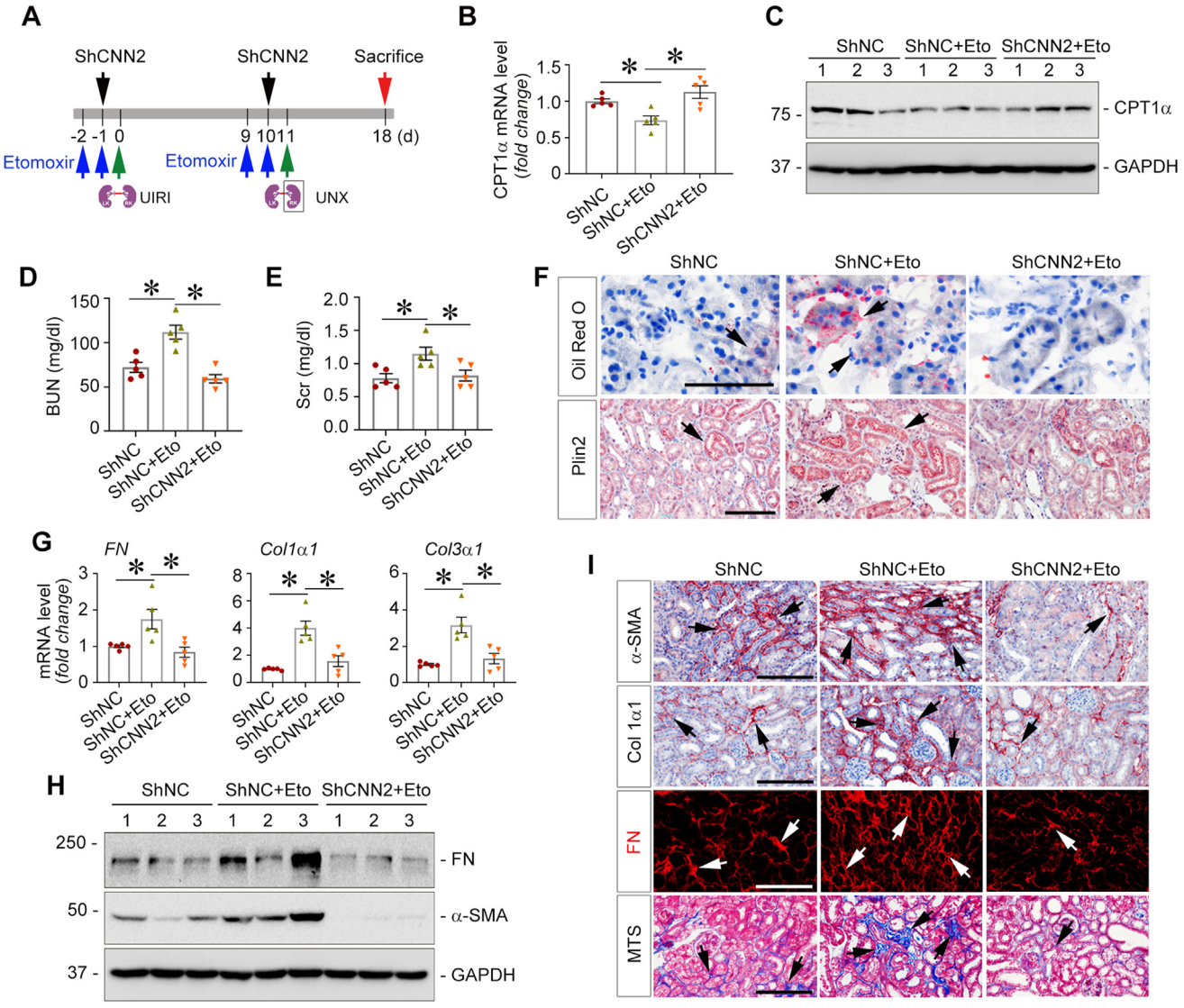

Figure 6: Knockdown of CNN2 enhances CPT1α activity to alleviate kidney fibrosis (**A**) Experiment design. CPT1α inhibitor, Etomoxir (Eto), was administrated in mice 2 days before unilateral IRI (UIRI) and nephrectomy (UNX), respectively. ShNC and ShCNN2 plasmids were injected at day (d) −1 and 10 through the tail vein. The mice were sacrificed on d18. (**B**) Quantitative RT-PCR (qPCR) analysis showed the changes of *CPT1α* mRNA levels in the fibrotic kidneys of ShNC mice, ShNC mice that received Etomoxir, and ShCNN2 mice that received Etomoxir after IRI. Graphs are presented as means ± SEM. $^*P < 0.05$ (n = 5). (**C**) Western blot assay demonstrated CPT1α protein expression in the fibrotic kidneys of ShNC mice, ShNC mice that received Etomoxir, and ShCNN2 mice that received Etomoxir after IRI. Numbers indicate individual animals within each group. (**D, E**) Blood urea nitrogen (BUN) and serum creatinine (Scr) levels in ShNC mice, ShNC mice that received Etomoxir, and ShCNN2 that received Etomoxir after IRI. Graphs are presented as means ± SEM. $^*P < 0.05$ (n = 5). (**F**) Representative micrographs for Oil Red O Staining and perilipin 2 (Plin2) immunohistochemical staining showed lipid accumulations in fibrotic kidneys of ShNC mice, ShNC mice that received Etomoxir, and ShCNN2 mice that received Etomoxir after IRI. Arrows indicate positive staining. Scale bar, 50 μm. (**G**) qPCR analyses revealed the mRNA abundance of *FN*, *α1 type I collagen*, and *α1 type III collagen* in the fibrotic kidneys of ShNC mice, ShNC mice that received Etomoxir, and ShCNN2 mice that received Etomoxir after IRI. Graphs are presented as means ± SEM. $^*P < 0.05$ (n = 5). (**H**) Western blot assay demonstrated FN and α-SMA proteins expression in the fibrotic kidneys of ShNC mice, ShNC mice that received Etomoxir, and ShCNN2 mice that received Etomoxir after IRI. Numbers indicate individual animals within each group. (**I**) Representative micrographs for immunostaining of α-SMA, Col1α1, fibronectin (FN), and Masson Trichrome Staining (MTS) showed myofibroblast activation and collagen deposition in the fibrotic kidneys of ShNC mice, ShNC mice that received Etomoxir, and ShCNN2 mice that received Etomoxir after IRI. Arrows indicate positive staining. Scale bar, 50 μm.

Figure S9E), but PPARα levels were increased in HK-2 cells after incubation with CNN2-deprived CM (Figure 7, K and M). Conversely, CNN2 recombinant protein repressed PPARα expression (Figure 7, L and N). However, knockdown of ESR2 abolished PPARα induction upon incubation with CNN2-deprived CM in HK2 cells (Figure 7O).

3.8. CNN2 knockdown in fibroblasts promotes FAO in tubular cells

To study how CNN2 regulates FAO in tubular cells, we incubated HK-2 with CNN2-deprived CM. qPCR analysis revealed that the key rate-limiting enzymes including *CPT1α*, *Acox1*, *Acsm1*, and *Acsm5* mRNA levels were induced by CNN2-deprived CM under TGF-β stress (Figure 8A). Consequently, CNN2-deprived CM reduced FN induction and inhibited α-SMA expression (Figure 8B). However, knockdown of ESR2 largely abolished induction of CPT1α, ACOX1, and Acsm1 and increased FN and α-SMA (Figure 8, C—D). To confirm that CNN2 mediates kidney fibrosis by affecting the FAO pathway in tubules, HK-2 cells were incubated with CNN2-deprived CM followed by etomoxir under TGF-β stress. Western blot assays demonstrated that etomoxir abolished the

 © 2023 The Author(s). Published by Elsevier GmbH. This is an open access article under the CC BY-NC-ND license (http://creativecommons.org/licenses/by-nc-nd/4.0/).

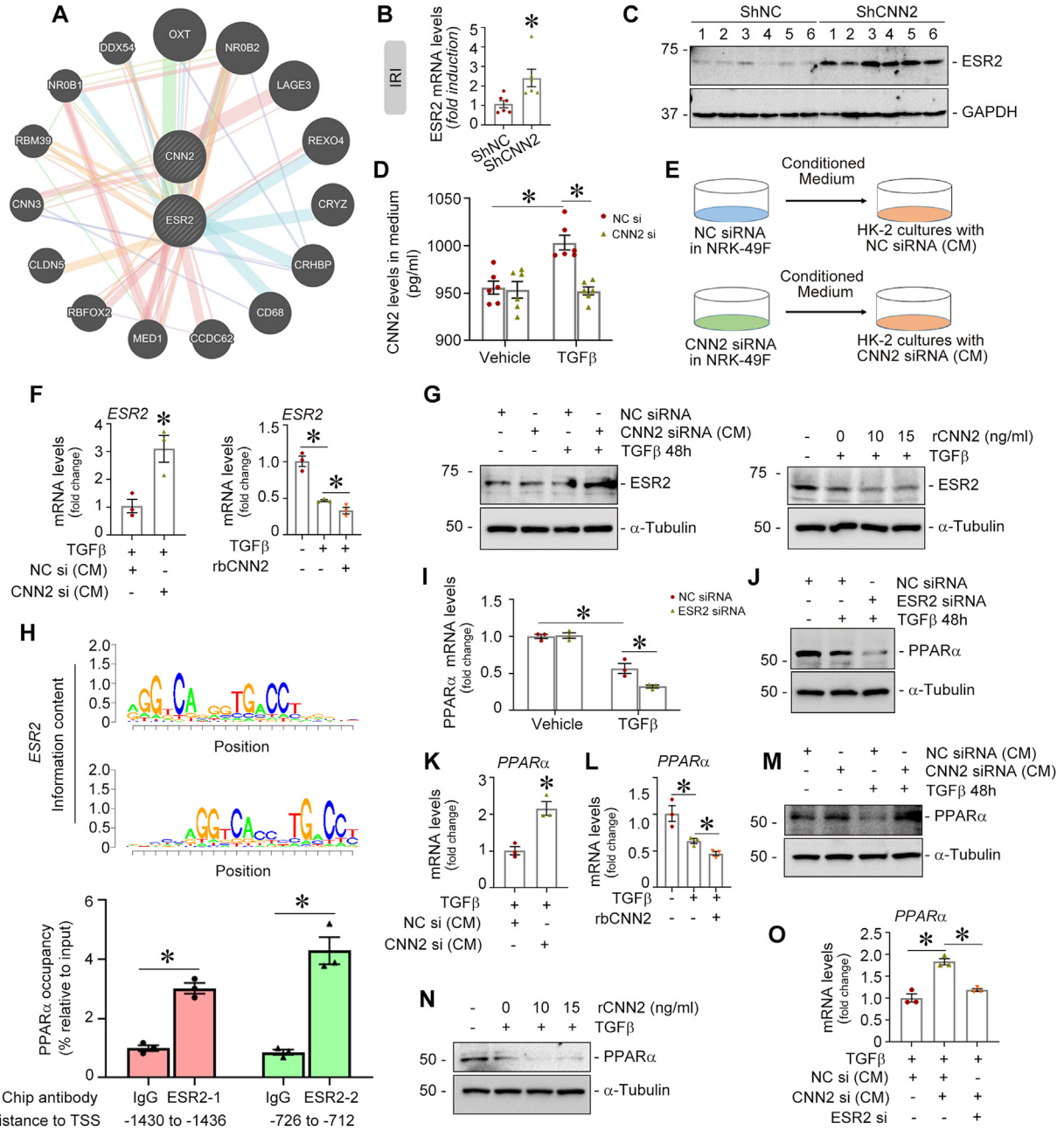

Figure 7: Knockdown of CNN2 promotes ESR2 binding PPARα to enhance fatty acid oxidation (**A**) Based on the GeneMANIA database, the human protein–protein interaction analysis showed CNN2 interacts with estrogen receptor 2 (ESR2). (**B**) Quantitative RT-PCR (qPCR) analysis showed the abundance of *ESR2* mRNA levels in ShNC and ShCNN2 mice fibrotic kidneys after IRI. Graphs are presented as means ± SEM. $^*P < 0.05$ (n = 6). (**C**) Western blot assay demonstrated ESR2 protein expression in the fibrotic kidneys of ShNC and ShCNN2 mice after IRI. Numbers indicate individual animals within each group. (**D**) ELISA showed CNN2 levels in the conditioned medium (CM) collected from the cultured fibroblasts after knockdown of CNN2 under TGF-β stress. Graphs are presented as means ± SEM. $^*P < 0.05$ (n = 6). (**E**) Schematic diagram showed CNN2-deprived CM from the cultured fibroblasts or recombinant CNN2 protein were employed to treat human kidney proximal tubular cells (HK-2). (**F**) qPCR showed *ESR2* expression in HK-2 cells after incubation with CNN2-deprived CM or human recombinant CNN2 protein. Graphs are presented as means ± SEM. $^*P < 0.05$ (n = 3). (**G**) Western blot assay demonstrated ESR2 expression in HK-2 cells after incubation with CNN2-deprived CM or human recombinant CNN2 protein. (**H**) ChIP-qPCR assay showed ESR2 binds to putative sequences in the promoter of *PPARα* genes. HK-2 cells were treated with ESR2 agonist (LY500307) for 3 h. Chromatin preparations from the cells were immunoprecipitated using an anti-ESR2 antibody, and co-precipitated DNA fragments were amplified using primers specific for the PPARα promoter. Graphs are presented as means ± SEM. $^*P < 0.05$ (n = 3). The upper panel showed representative DNA sequence logo representing the binding motif of the ESR2 gene. (**I**) qPCR analyses revealed the mRNA abundances of *PPARα* were reduced in HK-2 cells after knockdown of ESR2 under TGFβ1 stress, compared with scramble controls. Graphs are presented as means ± SEM. $^*P < 0.05$ (n = 3). (**J**) Western blot assay demonstrated that knockdown of ESR2 repressed PPARα expression in HK-2 cells under TGFβ1 stress, compared with scramble controls. (**K, L**) qPCR analyses revealed the mRNA abundances of *PPARα* were increased in HK-2 cells by CNN2-deprived CM (**K**) but were repressed by CNN2 recombinant protein (**L**) under TGFβ1 stress, compared with controls. Graphs are presented as means ± SEM. $^*P < 0.05$ (n = 3). (**M, N**) Western blot assays demonstrated that CNN2-deprived CM enhanced PPARα expression (**M**) but CNN2 recombinant protein repressed PPARα inductions (**N**) in HK-2 cells under TGFβ1 stress, compared with controls. (**O**) qPCR analyses revealed the mRNA abundances of *PPARα* were induced by CNN2-deprived CM but were repressed after knockdown of ESR2 under TGFβ1 stress. Graphs are presented as means ± SEM. $^*P < 0.05$ (n = 3).

 © 2023 The Author(s). Published by Elsevier GmbH. This is an open access article under the CC BY-NC-ND license (http://creativecommons.org/licenses/by-nc-nd/4.0/).

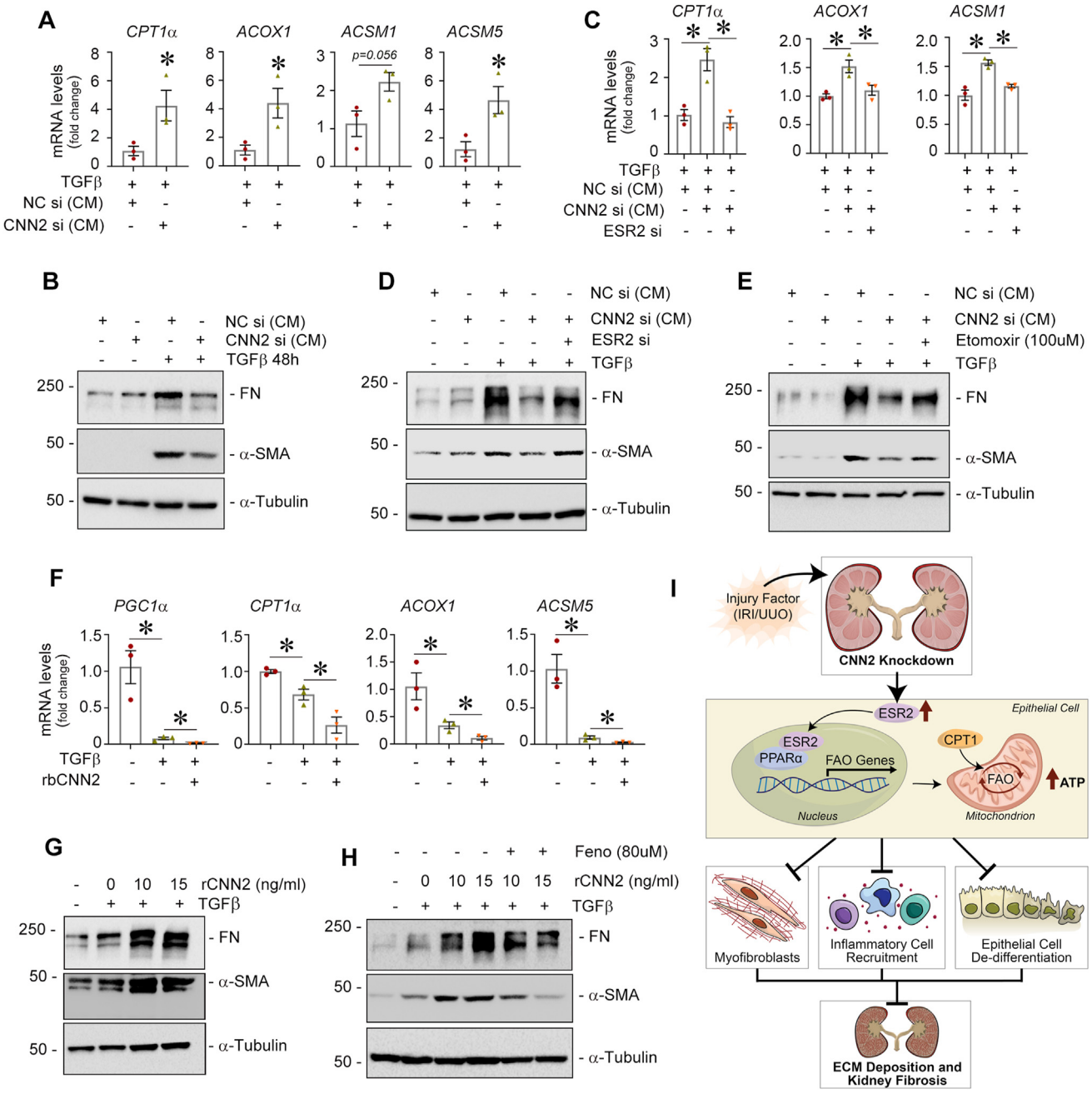

Figure 8: Knockdown of CNN2 alleviates defective fatty acid oxidation and ECM deposition in tubular cells. (**A**) qPCR analyses revealed the mRNA abundances of *CPT1α*, *ACOX1, Acsm1,* and *Acsm5* were increased in HK-2 cells incubated with CNN2-deprived CM under TGFβ1 stress, compared with controls. Graphs are presented as means ± SEM. $^*P < 0.05$ (n = 3). (**B**) Western blot assay demonstrated that CNN2-deprived CM reduced the inductions of FN and α-SMA in HK-2 cells under TGFβ1 stress, compared with controls. (**C**) qPCR analyses revealed the mRNA abundances of *CPT1α*, *ACOX1,* and *Acsm1* were increased by CNN2-deprived CM in HK-2 cells but were repressed after knockdown of ESR2 under TGFβ1 stress, compared with controls. Graphs are presented as means ± SEM. $^*P < 0.05$ (n = 3). (**D**) Western blot assays demonstrated CNN2-deprived CM alleviated FN and α-SMA inductions in HK-2 cells under TGFβ1 stress but they were increased after knockdown of ESR2, compared with controls. (**E**) Under TGFβ1 stress, HK-2 cells were incubated with CNN2-deprived CM and followed by CPT1α inhibitor Etomoxir (100 μM). Western blot assays showed Etomoxir induced FN and α-SMA expression after incubation with CNN2-deprived CM. (**F**) qPCR analyses revealed the mRNA abundances of *PGC1α, CPT1α, ACOX1,* and *Acsm5* were reduced in HK-2 cells incubated with CNN2 recombinant protein under TGFβ1 stress. Graphs are presented as means ± SEM. $^*P < 0.05$ (n = 3). (**G**) Western blot assay demonstrated that CNN2 recombinant induced FN and α-SMA expression in HK-2 cells after TGFβ1 stimulations. (**H**) Under TGFβ1 stress, HK-2 cells were treated with CNN2 recombinant proteins followed by PPARα agonist Fenofibrate (Feno, 80 μM). Western blot assays showed Fenofibrate decreased FN and α-SMA expression after treated with CNN2 recombinant protein. (**I**) Schematic diagram depicts knockdown of CNN2 promotes ESR2 binding to PPARα to transcriptionally regulate the FAO genes to halt kidney fibrosis.

 © 2023 The Author(s). Published by Elsevier GmbH. This is an open access article under the CC BY-NC-ND license (http://creativecommons.org/licenses/by-nc-nd/4.0/).

beneficial effects of CNN2-deprived CM on reducing induction of FN and α-SMA (Figure 8E). In comparison, HK-2 cells treated with human recombinant CNN2 protein repressed mRNA levels of *PGC1α*, *CPT1α*, *Acox1*, and *Acsm5* after TGF-β stimulation (Figure 8F). Similarly, CNN2 recombinant protein increased FN and α-SMA induction (Figure 8G). In a separate experiment, HK-2 cells were treated with CNN2 recombinant protein followed by the PPARα agonist, fenofibrate. After stimulation with TGF-β, western blots demonstrated that fenofibrate ameliorated CNN2-induced FN and α-SMA *in vitro* (Figure 8H).

4. DISCUSSION

This study elucidated CKD pathogenesis from the perspective of cellular mechanics and metabolism interactions (Figure 8I). We demonstrated that CNN2, a prominent actin stabilizer, determines kidney fibrosis through modulating FA metabolism as evident by: 1) knockdown of CNN2 alleviated kidney fibrosis in CKD models; 2) if the FAO pathway was activated, then less lipid accumulated in ShCNN2 fibrotic kidneys; 3) knockdown of CNN2 preserved kidney functions after inhibiting the key rate-limiting enzyme, CPT-1α; 4) CNN2's interactor, ESR2, transcriptionally mediates the regulator of the FAO pathway, PPARα; and 5) serum CNN2 is increased in CKD patients. These results provide rationale for expanding the paradigm of mechano-metabolic programming after CKD.

In mice and human fibrotic kidneys, CNN2 is mainly expressed in interstitial fibroblasts or pericytes (Figure 2). CNN2 possesses the capacity of generating significant forces when fibroblasts/pericytes communicate with the neighboring cells due to its nature as an actin filament regulatory protein. It directly determines the extent of kidney fibrosis by forming a deleterious kidney local microenvironment (KLM). Due to mechanical changes in a fibrotic kidney, injured kidney cells receive information from the microenvironment to coordinate their behavior at local and systemic levels. Our results indicate that CNN2 affects both levels in CKD. At the local level, it serves as an actin stabilizer. Under physiological conditions, CNN2 controls cell shape, polarity, migration, and establishes intercellular contacts to support organ architecture [5]. After CKD, fibrotic niche-like KLM formation is a critical structural change in kidneys [29]. The densities, sizes, and cellular/non-cellular components of niches determine the severity of kidney fibrosis. Amid these processes, all kidney cells experience pathological external forces. These highly varied forces may mediate individual cell phenotypes and kidney architecture changes [4]. Our data show that knockdown of CNN2 alleviates kidney fibrosis after ischemic and obstructive CKD (Figure 3 and Supplementary Figure S2). From the aspect of mechanical changes, dysregulated CNN2 reduces the injured cells' ability to quickly reinforce their mechanosensitive structures and cytoskeleton so they do not respond to forces appropriately. After CKD, actin cytoskeleton disarrangement causes aberrant activation of fibroblasts, excessive ECM deposition, and tubular atrophy which lead to the irreversible change of KLM. At the systemic level, CNN2 is able to mediate mechanical and chemical signal interactions. It is reported that rapid CNN2 degradation is required for cytokines to inhibit malignant tumor growth [35]. A recent study also indicated that CNN2 could be ubiquitylated and removed for efficient lysophagy during lysosomal membrane permeabilization [36]. As well, CNN2 was increased in CKD patients' serum (Figure 2). Therefore, CNN2 may also enter the KLM via the bloodstream, regulating cell behavior to maintain the forces in the kidney fibrotic regions. In addition, CNN2 expression is associated with LDL-C levels in stage 2 CKD patients (Data not shown). This phenomenon leaves us questioning, does CNN2 affect lipid or FA metabolism reprogramming in fibrotic kidneys?

Metabolic reprogramming is a hallmark of malignant transformation [37]. This process includes activating signal transduction cascades, key metabolic enzymes, and transcriptional regulation of genes encoding metabolic enzymes [38]. Although the interaction between the actin cytoskeleton and metabolic enzymes was observed decades ago [39], most studies investigating cellular mechanics remain focused on supporting organ architecture rather than metabolic reprogramming. As a highly metabolically active organ [40], kidney metabolism is markedly disturbed after CKD (Figure 1). Our proteomics data suggest that all metabolic pathways, including FA, carbohydrates, and amino acids, and about 40 FAO-related enzymes were upregulated in ShCNN2 kidneys (Figure 4). Specifically, gene expression of the key regulators of FAO (*PPARα*) and rate-limiting enzymes (*Acsm1, 2, 5*, *CPT1α*, *Acox1-3*, *Acadm*, *Acadl*, and *Acad10*) were upregulated in ShCNN2 kidney TECs. Although CNN2 is predominantly expressed in fibroblasts/pericytes, communication between TECs and fibroblasts in the KLM is critical in determining the severity of CKD [41]. As the largest cell population of kidneys, TECs are not bystanders in kidney fibrosis [29]. TECs are the main energy consuming cells, and FAO is their chief ATP source in kidneys. Lower FAO in TECs, followed by intracellular lipid accumulation, profoundly switches TECs into a pro-fibrotic phenotype and leads to kidney fibrosis [42,43]. Indeed, intracellular triglyceride levels were reduced in ShCNN2 kidneys after CKD (Figure 6 and Supplementary Figure S7). Most importantly, after systemic knockdown of CNN2 *in vivo*, liver triglyceride and FAO genes have minor changes between ShNC and ShCNN2 mice after IRI-induced CKD although the liver is the central organ in maintaining lipid homeostasis (Supplementary Figure S6). Therefore, we speculated that CNN2 independently regulates intra-renal lipid accumulation and the FAO pathway activation by mediating cellular mechanical and chemical signals. CNN2 knockdown rescued CPT1α inhibitor-induced kidney fibrosis by stimulating FA import into the mitochondria and initiating mitochondrial fission. Enhanced FAO provides more ATP to maintain the structural integrity of actin filaments.

The most novel finding of this study is that ESR2 is a bridge that connects CNN2 and PPARα to modulate FAO after CKD (Figure 7), which we determined via several lines of evidence. First, ESR2 interacts with CNN2. Second, as a nuclear transcription factor, ESR2 harbors similar conserved sequences with PPARα in its promoter regions, and ESR2 agonist promotes their binding. Third, CNN2 knockdown alleviated kidney fibrosis, whereas knockdown of both CNN2 and ESR2 abolished these protective effects and repressed FAO. Consistent with the protective role of ESR2 in cancer, neuropathies, cardiovascular disease, osteoporosis, menopause, and metabolic disorders [44], the finding that CNN2 controls ESR2 to influence FAO and kidney fibrosis provides new insight into how mechanical signals contribute to CKD development; although, FAO is positioned at the intersection of multiple chemical signals such as TGF-β, Krüppel-like factor 15, and CD36 [45–47]. Of note, in our *in vitro* system, whether the employed conditioned medium contains other soluble or transferrable factors such as a PPARα activating factor to mediate the FAO pathway needs to be determined.

Despite the robust evidence that demonstrates how the actin stabilizer CNN2 regulates metabolism, several unanswered questions remain. First, could CNN2 in T-cells be equally important to its role in fibroblasts/pericytes during kidney disease progression after IRI? Our deconvolution analysis in Figure 2F indicates it may be important; however, the exact role of CNN2 expression in immune cells and how this mediates kidney fibrosis remains unclear. Second, does altered glucose metabolism contribute to kidney fibrosis in ShCNN2 kidneys, given that kidneys are important for glucose reabsorption, production, and utilization? Third, as we did not generate CNN2 genetic mouse

 © 2023 The Author(s). Published by Elsevier GmbH. This is an open access article under the CC BY-NC-ND license (http://creativecommons.org/licenses/by-nc-nd/4.0/).

models, would genetic knockout of CNN2 have the same effects *in vivo*?

In summary, our investigation of cellular mechanics and metabolism interactions identified that the knockdown of actin stabilizer, CNN2, alleviated kidney fibrosis by activating FA metabolism. The new insights on modulating cellular mechanical properties to tune energy production in response to formation of the kidney fibrotic microenvironment supplement our understanding of CKD pathogenesis. The possibility of employing approaches to target mechano-metabolic mechanisms may shed light on treating CKD.

AUTHOR CONTRIBUTIONS

Conceptualization, Y.G. and D.Z.; methodology, Y.G., J.T., S.B., H.F., and D.Z.; investigation, Y.G., Y.W., Z.P., J.W., P.G., Y.Q., and Y.Y.; writing — original draft, Y.G. and D.Z.; writing — review& editing, Y.G., D.K., S.L., Y.W., and D.Z.; funding acquisition, D.Z.; resources and supervision, D.Z.

DATA AVAILABILITY

Data will be made available on request.

ACKNOWLEDGMENTS

This work was supported by the National Institutes of Health (NIH) grants DK116816, DK128529, and DK132059. We are grateful to Dr. Benjamin Humphreys lab at Washington University in St. Louis for using their online database and Dr. Justin D. Radolf at the University of Connecticut, School of Medicine for reviewing the manuscript.

CONFLICT OF INTEREST

We declared that none of the authors has conflict of interest.

APPENDIX A. SUPPLEMENTARY DATA

Supplementary data to this article can be found online at https://doi.org/10.1016/j.molmet.2023.101712.

REFERENCES

[1] Foreman KJ, Marquez N, Dolgert A, Fukutaki K, Fullman N, McGaughey M, et al. Forecasting life expectancy, years of life lost, and all-cause and cause-specific mortality for 250 causes of death: reference and alternative scenarios for 2016-40 for 195 countries and territories. Lancet 2018;392:2052—90.

[2] Kalantar-Zadeh K, Jafar TH, Nitsch D, Neuen BL, Perkovic V. Chronic kidney disease. Lancet 2021;398:786—802.

[3] Li L, Fu H, Liu Y. The fibrogenic niche in kidney fibrosis: components and mechanisms. Nat Rev Nephrol 2022;18:545—57.

[4] Wells RG. Tissue mechanics and fibrosis. Biochim Biophys Acta 2013;1832:884—90.

[5] DeWane G, Salvi AM, DeMali KA. Fueling the cytoskeleton - links between cell metabolism and actin remodeling. J Cell Sci 2021;134.

[6] Liu R, Jin JP. Calponin isoforms CNN1, CNN2 and CNN3: regulators for actin cytoskeleton functions in smooth muscle and non-muscle cells. Gene 2016;585:143—53.

[7] Moazzem Hossain M, Wang X, Bergan RC, Jin JP. Diminished expression of h2-calponin in prostate cancer cells promotes cell proliferation, migration and the dependence of cell adhesion on substrate stiffness. FEBS Open Bio 2014;4:627—36.

[8] Hu J, Xie W, Shang L, Yang X, Li Q, Xu M, et al. Knockdown of calponin 2 suppressed cell growth in gastric cancer cells. Tumour Biol 2017;39:1010428317706455.

[9] Huang QQ, Hossain MM, Sun W, Xing L, Pope RM, Jin JP. Deletion of calponin 2 in macrophages attenuates the severity of inflammatory arthritis in mice. Am J Physiol Cell Physiol 2016;311:C673—85.

[10] Plazyo O, Liu R, Moazzem Hossain M, Jin JP. Deletion of calponin 2 attenuates the development of calcific aortic valve disease in ApoE(-/-) mice. J Mol Cell Cardiol 2018;121:233—41.

[11] Hsieh TB, Feng HZ, Jin JP. Deletion of calponin 2 reduces the formation of postoperative peritoneal adhesions. J Invest Surg 2022;35:517—24.

[12] Kang X, Wang F, Lan X, Li X, Zheng S, Lv Z, et al. Lentivirus-mediated shRNA targeting CNN2 inhibits hepatocarcinoma in vitro and in vivo. Int J Med Sci 2018;15:69—76.

[13] Evers TMJ, Holt LJ, Alberti S, Mashaghi A. Reciprocal regulation of cellular mechanics and metabolism. Nat Metab 2021;3:456—68.

[14] Li Y, Sha Z, Peng H. Metabolic reprogramming in kidney diseases: evidence and therapeutic opportunities. Internet J Nephrol 2021;2021:5497346.

[15] Tran MT, Zsengeller ZK, Berg AH, Khankin EV, Bhasin MK, Kim W, et al. PGC1alpha drives NAD biosynthesis linking oxidative metabolism to renal protection. Nature 2016;531:528—32.

[16] Bays JL, Campbell HK, Heidema C, Sebbagh M, DeMali KA. Linking E-cadherin mechanotransduction to cell metabolism through force-mediated activation of AMPK. Nat Cell Biol 2017;19:724—31.

[17] Console L, Scalise M, Giangregorio N, Tonazzi A, Barile M, Indiveri C. The link between the mitochondrial fatty acid oxidation derangement and kidney injury. Front Physiol 2020;11:794.

[18] Miguel V, Tituana J, Herrero JI, Herrero L, Serra D, Cuevas P, et al. Renal tubule Cpt1a overexpression protects from kidney fibrosis by restoring mitochondrial homeostasis. J Clin Invest 2021;131.

[19] Kang HM, Ahn SH, Choi P, Ko YA, Han SH, Chinga F, et al. Defective fatty acid oxidation in renal tubular epithelial cells has a key role in kidney fibrosis development. Nat Med 2015;21:37—46.

[20] Han SH, Wu MY, Nam BY, Park JT, Yoo TH, Kang SW, et al. PGC-1alpha protects from notch-induced kidney fibrosis development. J Am Soc Nephrol 2017;28:3312—22.

[21] Khan S, Cabral PD, Schilling WP, Schmidt ZW, Uddin AN, Gingras A, et al. Kidney proximal tubule lipoapoptosis is regulated by fatty acid transporter-2 (FATP2). J Am Soc Nephrol 2018;29:81—91.

[22] Baek J, He C, Afshinnia F, Michailidis G, Pennathur S. Lipidomic approaches to dissect dysregulated lipid metabolism in kidney disease. Nat Rev Nephrol 2022;18:38—55.

[23] Iwai N, Katsuya T, Mannami T, Higaki J, Ogihara T, Kokame K, et al. Association between SAH, an acyl-CoA synthetase gene, and hypertriglyceridemia, obesity, and hypertension. Circulation 2002;105:41—7.

[24] Szeto HH. Pharmacologic approaches to improve mitochondrial function in AKI and CKD. J Am Soc Nephrol 2017;28:2856—65.

[25] He M, Pei Z, Mohsen AW, Watkins P, Murdoch G, Van Veldhoven PP, et al. Identification and characterization of new long chain acyl-CoA dehydrogenases. Mol Genet Metabol 2011;102:418—29.

[26] Jang HS, Noh MR, Kim J, Padanilam BJ. Defective mitochondrial fatty acid oxidation and lipotoxicity in kidney diseases. Front Med 2020;7:65.

[27] Chau BN, Xin C, Hartner J, Ren S, Castano AP, Linn G, et al. MicroRNA-21 promotes fibrosis of the kidney by silencing metabolic pathways. Sci Transl Med 2012;4:121ra118.

[28] Zhou D, Liu Y. Renal fibrosis in 2015: understanding the mechanisms of kidney fibrosis. Nat Rev Nephrol 2016;12:68—70.

[29] Fu H, Gui Y, Liu S, Wang Y, Bastacky SI, Qiao Y, et al. The hepatocyte growth factor/c-met pathway is a key determinant of the fibrotic kidney local microenvironment. iScience 2021;24:103112.

 © 2023 The Author(s). Published by Elsevier GmbH. This is an open access article under the CC BY-NC-ND license (http://creativecommons.org/licenses/by-nc-nd/4.0/).

[30] Zhou D, Wang Y, Gui Y, Fu H, Zhou S, Wang Y, et al. Non-canonical Wnt/calcium signaling is protective against podocyte injury and glomerulosclerosis. Kidney Int 2022;102:96–107.
[31] Lin YH, Platt MP, Fu H, Gui Y, Wang Y, Gonzalez-Juarbe N, et al. Global proteome and phosphoproteome characterization of sepsis-induced kidney injury. Mol Cell Proteomics 2020;19:2030–47.
[32] Kirita Y, Wu H, Uchimura K, Wilson PC, Humphreys BD. Cell profiling of mouse acute kidney injury reveals conserved cellular responses to injury. Proc Natl Acad Sci U S A 2020;117:15874–83.
[33] Sztalryd C, Brasaemle DL. The perilipin family of lipid droplet proteins: gatekeepers of intracellular lipolysis. Biochim Biophys Acta Mol Cell Biol Lipids 2017;1862:1221–32.
[34] Li H, Dixon EE, Wu H, Humphreys BD. Comprehensive single-cell transcriptional profiling defines shared and unique epithelial injury responses during kidney fibrosis. Cell Metabol 2022;34:1977–1998 e1979.
[35] Qian A, Hsieh TB, Hossain MM, Lin JJ, Jin JP. A rapid degradation of calponin 2 is required for cytokinesis. Am J Physiol Cell Physiol 2021;321:C355–68.
[36] Kravic B, Bionda T, Siebert A, Gahlot P, Levantovsky S, Behrends C, et al. Ubiquitin profiling of lysophagy identifies actin stabilizer CNN2 as a target of VCP/p97 and uncovers a link to HSPB1. Mol Cell 2022;82:2633–2649 e2637.
[37] Faubert B, Solmonson A, DeBerardinis RJ. Metabolic reprogramming and cancer progression. Science 2020;368.
[38] Park JS, Burckhardt CJ, Lazcano R, Solis LM, Isogai T, Li L, et al. Mechanical regulation of glycolysis via cytoskeleton architecture. Nature 2020;578:621–6.
[39] Poglazov BF, Livanova NB. Interaction of actin with the enzymes of carbohydrate metabolism. Adv Enzym Regul 1986;25:297–305.
[40] Gewin LS. Sugar or fat? Renal tubular metabolism reviewed in Health and disease. Nutrients 2021;13.
[41] Gewin L, Zent R, Pozzi A. Progression of chronic kidney disease: too much cellular talk causes damage. Kidney Int 2017;91:552–60.
[42] Xu S, Jia P, Fang Y, Jin J, Sun Z, Zhou W, et al. Nuclear farnesoid X receptor attenuates acute kidney injury through fatty acid oxidation. Kidney Int 2022;101:987–1002.
[43] Idowu TO, Parikh SM. A new chapter in lipid signaling and kidney fibrosis. Sci Transl Med 2022;14:eadd2826.
[44] Paterni I, Granchi C, Katzenellenbogen JA, Minutolo F. Estrogen receptors alpha (ERalpha) and beta (ERbeta): subtype-selective ligands and clinical potential. Steroids 2014;90:13–29.
[45] Piret SE, Attallah AA, Gu X, Guo Y, Gujarati NA, Henein J, et al. Loss of proximal tubular transcription factor Kruppel-like factor 15 exacerbates kidney injury through loss of fatty acid oxidation. Kidney Int 2021;100:1250–67.
[46] Liu H, Chen YG. The interplay between TGF-beta signaling and cell metabolism. Front Cell Dev Biol 2022;10:846723.
[47] Hao JW, Wang J, Guo H, Zhao YY, Sun HH, Li YF, et al. CD36 facilitates fatty acid uptake by dynamic palmitoylation-regulated endocytosis. Nat Commun 2020;11:4765.

 © 2023 The Author(s). Published by Elsevier GmbH. This is an open access article under the CC BY-NC-ND license (http://creativecommons.org/licenses/by-nc-nd/4.0/).